ISSN 0016-8521, Geotectonics, 2014, Vol. 48, No. 1, pp. 68–85. © Pleiades Publishing, Inc., 2014.
Original Russian Text © M.D. Khutorskoi, B.G. Polyak, 2014, published in Geotektonika, 2014, Vol. 48, No. 1, pp. 77–96.

Geothermal Models of Various Geodymanic Settings

M. D. Khutorskoi and B. G. Polyak

Geological Institute, Russian Academy of Sciences, Pyzhevskii per. 7, Moscow, 119017 Russia
e-mail: mkhutorskoy@ginras.ru

Received April 15, 2013.

Abstract—The distribution of heat flow, deep temperature, and helium isotope ratios in axial spreading zones of mid-ocean ridges and in scattered spreading zones in backarc basins are considered, as well as in active segments of transform fracture zones, intra- and pericontinental rift zones, linear and mosaic Paleozoic foldbelts, and loading and extension sedimentary basins. The heat flow in these structural elements varies widely from 15 to 1500 mW/m^2, and the thickness of the thermal lithosphere is correspondingly variable. The quantitatively estimated radiogenic heat generation in Paleozoic foldbelts provides 40–50% of the background heat flow. A time-dependent heat flow is characteristic of not only recent but also Late Paleozoic tectonic belts. The origin of positive and negative geothermal anomalies has been explained. Localization of hydrocarbon fields in sedimentary basins is linked to these anomalies.

DOI: 10.1134/S0016852114010026

INTRODUCTION

Heat flow density[1] from the Earth's interior is an important indicator of current and past geodynamic activity of lithospheric structural units.

Knowing a thermophysical structure of geological section, one can calculate the position of geotherms in the Earth's crust and upper mantle; compare this section with the thermodynamic conditions of metamorphism, the phase state of matter, and magnetization of rocks; and localize zones of sharp lateral temperature contrasts, as a rule, controlling seismic and magmatic activity. Therefore, quantitative interpretation of geothermal data (geothermal simulation) is a powerful tool for understanding the structure of the lithosphere in various geodynamic settings.

Rift zones, foldbelts, and sedimentary basins are characterized by specific attributes of volcanism, metamorphism, and metallogeny, as well as by anomalies of potential geophysical fields, including the geothermal field, which are variable in shape, ~~sense~~, and intensity.

This paper is concerned just with geothermal fields. The distributions of heat flow and deep temperature in oceanic and continental rift zones, linear and mosaic foldbelts, and loading and extension sedimentary basins are considered from literature sources and the results of our own measurements carried out in various regions of the World Ocean and northern Eurasia.

[1] Instead of conductive heat flow density as a vectorial characteristic of the Earth's thermal field, the term *heat flow* is used below, always implying its density.

RECENT RIFT ZONES

Rifts are formed on continents and in oceans in different geodynamic settings of active or passive rifting [58]. This terminology attaches much more importance to similar consequences of the newly formed crust spreading in oceans and destruction of the ancient crust on continents rather than to the difference in the mechanisms of these processes, which is more important for understanding their origin.

~~*Mid-ocean rifts (zones of axial spreading).*~~ As is known, anomalously high, as well as zeroth and even negative, values of conductive heat flow density were revealed in the rift basins along axes of mid-ocean ridges (MORs). The MORs are divergent plate boundaries, where spreading of the oceanic bottom occurs as a result of mantle material ~~emplacement~~. Therefore, the observed heat flow is determined not only by conductive but also convective efflux of heat. Rift basins develop along MOR axes, and their width is inversely proportional to the spreading rate. The conductive component of heat flow in these basins reaches values 15–30 times higher than the global mean. When ridge axes are overlapped, as, like in the California Bay or Red Sea, by a thick sedimentary cover, which prevents discharge of magma and thermal waters on the bottom, the measured conductive flow locally exceeding 1500 mW/m^2 is equivalent to the total heat loss, because in these cases, the convective component is close to zero. Under other conditions, when the thickness of sedimentary rocks is small, the measured conductive heat flow can be zero and even negative above the low-angle fault, along which hydrothermal solutions are being discharged. This, however, does not imply that heat is not removed from the lithosphere at this place. It is merely moved away by convection at

the almost zeroth or not higher than adiabatic value (0.4 mW/m^2) of conductive heat flow inside ascending convective (more precisely, advective) stream. At the same time, the average total heat loss calculated as the sum of the conductive and convective components remains of the same order of magnitude in various segments of oceanic ridges and, according to the available estimates, it ranges from 400 to 700 mW/m^2 [11, 44]. Approximately the same figures were yielded by calculation of total heat loss in rift zones of Iceland with allowance for hydrothermal solution discharge [40].

The amount of heat transferred by convection related to vertical magma filtration in the asthenosphere is ~~approximately~~ $Q \approx \rho c_p j T$, where j is the vertical filtration rate (~2×10^{-10} m/s); ρ is the magma density (2800 kg/m^3); c_p is the specific heat capacity of magma at constant pressure (1050 J/kg K); and T is its temperature (1300°C). At those parameters, the convective efflux of heat is estimated at $Q \approx 800$ mW/m^2. If the total filtration heat ~~flow~~ is concentrated in a narrow axial zone of a magmatic reservoir ~10 km in width, where magma pours from a wider 100-km asthenospheric domain owing to the centripetal horizontal component of filtration, then the total heat flow in the rift zone approximately fits those anomalous values measured in the California Bay and Red Sea.

Nearly orthogonal **transform fracture zones** (TFZs) with a prevalent shear component are genetically related to axial spreading zones. The geothermal state of TFZs remains poorly studied as compared with axial MOR zones; however, some of them (Atlantis, Kane, Vema ~~TFZ~~) are characterized by sufficiently complete data [44, 62, 68, 85].

~~The Vema TFZ~~ (~11° N) is an alternation of ~~sea-mounts (~~ridge blocks~~)~~ and depressions (latitudinal fractures) along which a segment of MAR located to the north has slipped westward by almost 3° in longitude. The depressions are filled with Pleistocene turbidites up to a kilometer in thickness [65].

The heat flow distribution in depressions and ridge blocks is quite different. In blocks, the distribution is typical of MAR and demonstrates a rather wide range of heat flow from 9 to 100 mW/m^2, although the average values in northern and southern blocks are approximately equal (59 and 51 mW/m^2, respectively at $1\sigma \approx$ 31 mW/m^2). The latitudinal depressions are distinguished by relatively stable and anomalously high heat flow (112–260 mW/m^2) at the mean value and standard deviation of 152 and 41 mW/m^2, respectively. Taking into account the screening effect of sedimentation on the thermal field [70], the deep flow in depressions is estimated at 250 mW/m^2 [44].

The heat flow in this and other TFZs is always anomalously high in their active parts (135–360 mW/m^2); negative values have not been established here. The heat flow in these parts of TFZs is characterized by stability and low dispersion. This implies that convective heat loss, which sharply disturbs the heat flow in axial zone of MOR, is not crucial

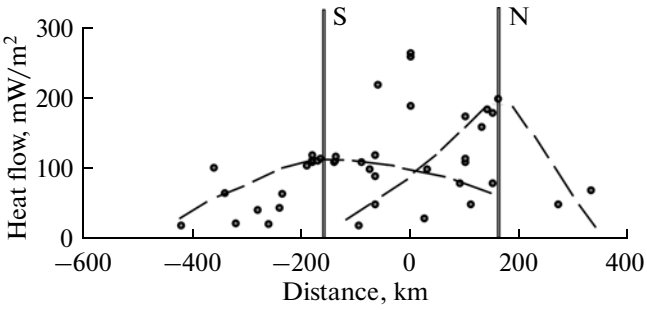

Fig. 1. Heat flow distribution along strike of latitudinal Vema TFZ. Dashed lines indicate position of the MAR axes to north (N) and south (S) of the TFZ. The zeroth mark on x-axis corresponds to center of active TFZ segment.

for TFZ. Indeed, most troughs in large TFZs are filled with thick (up to a kilometer) sedimentary sequences, and this rules out convection. As expeditions with deep-water submersibles have shown, even the 30–50-m layer of pelagic oozes is an impermeable screen for discharge of hydrothermal solutions from under them [86]. This gives the objective possibility of estimating the complete removal of energy in axial zones of rifts at their intersection with TFZs (see above).

Several mechanisms were discussed to explain anomalously high heat flow values in active parts of TFZs, for example, release of friction heat in zones of shearing. Frictional heating of the contacts between shifting blocks is inevitable. However, calculations for a number of TFZs, including the most reliable estimate this effect for the San Andreas Fault [74], have shown that the heat from tectonic friction does not play an appreciable role in the formation of the observed heat flow, providing no more than 15% of the measured value.

The model of superposed thermal anomalies [75] is currently popular. The heat flow anomaly for the Vema TFZ has been calculated as a result of superposition of fields related to the northern and southern walls of TFZ, which have different ages depending on the position of rift zone axes. This idea is substantiated in Fig. 1. The background conductive heat flow at the center of the active TFZ segment is determined as the sum of its values in the enveloping curves describing heat flow distribution across the strike of the southern and northern MAR segments (dashed lines). At the intersection point, the heat flow is 110 mW/m^2, and thus the total is 220 mW/m^2. This value is consistent with estimates from other models. The anomalously high heat flow in the active TFZ part (250–270 mW/m^2) is apparently caused by heat supply due to its convective discharge on the exposed ridge blocks.

Backarc basins of marginal seas (scattered spreading zones). Spreading of the sea bottom as a result of mantle material discharge develops not only in oceans but also in almost all backarc marginal seas. In partic-

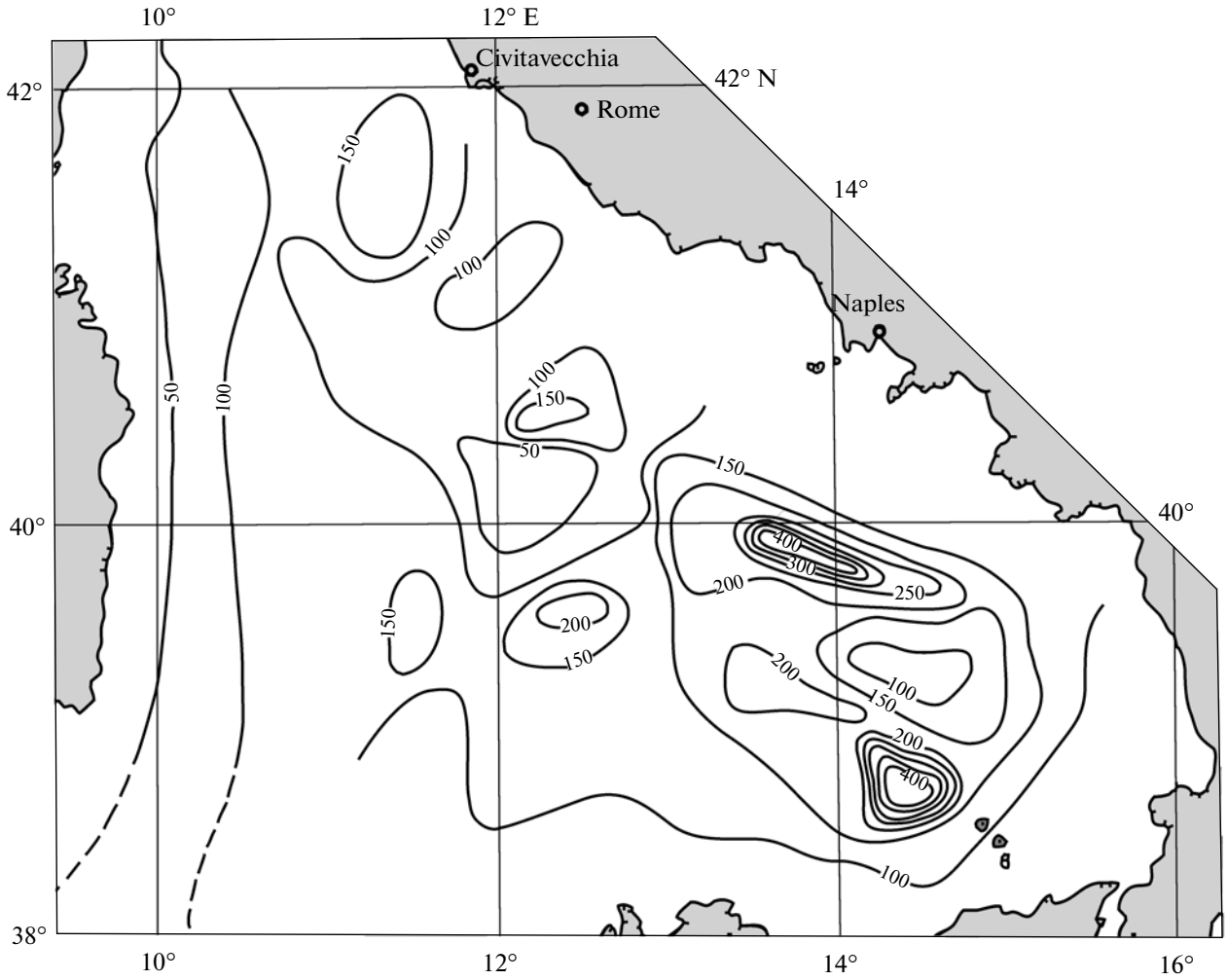

Fig. 2. Map of heat flow in Tyrrhenian Sea. Contour lines are given in mW/m^2, modified after [67].

ular, it is strikingly expressed and well-studied in terms of geothermics in the Tyrrhenian Sea.

As follows from geophysical data and results of deep sea drilling [60], the Mesozoic Paleotyrrhenian basin with oceanic crust had been completely subducted beneath Sardinia by the onset of Tortonian. The recent Tyrrhenia was formed as a marginal basin behind the Late Neogene Calabrian arc [64]. Calc-alkaline volcanism in the Lipari island arc was ascribed to the subduction zone plunging to the west [60], whereas the 200-m sequence of MORB-type olivine tholeiites penetrated by DSDP holes 373 and 373a in center of the Tyrrhenian Sea was related to scattered spreading. This reflects the different geodynamic settings in distinct parts of the Tyrrhenian Basin. The western part was characterized by compressive stresses from the Tortonian and until now, whereas the eastern part was affected by tensile stresses over the same 11 Ma. The eastern part of the Tyrrhenian Sea is a region of high heat flow, large lateral temperature gradients, and submarine basaltic volcanism (Fig. 2). The highest values of heat flow (515 and 490 mW/m^2) have been measured in the backarc zone of the Lipari island arc against a mean background value of 155 mW/m^2 in this part of the sea [66]. The thickness of the thermal lithosphere in the eastern Tyrrhenian Sea is 17–23 km [54] (Fig. 3).

The high heat flow, basaltic volcanism, and small thickness of the lithosphere in the Tyrrhenian Sea are evidence for ~~emplacement~~, of mantle material, which ~~wedged out~~, previously existing blocks. The same is indicated by a high gravity anomaly (> 200 mGal in Bouguier reduction) above the Vavilov massif in the eastern Tyrrhenian Sea [81].

Intracontinental rift zones similar in morphology to axial MOR rifts markedly differ from them in origin and heat ~~removal~~, which is appreciably higher than the average level in adjacent regions. The thermal field of these structural units is discussed in many publications. The most complete characterization was presented by Lysak [23], whose data are summarized in Table 1.

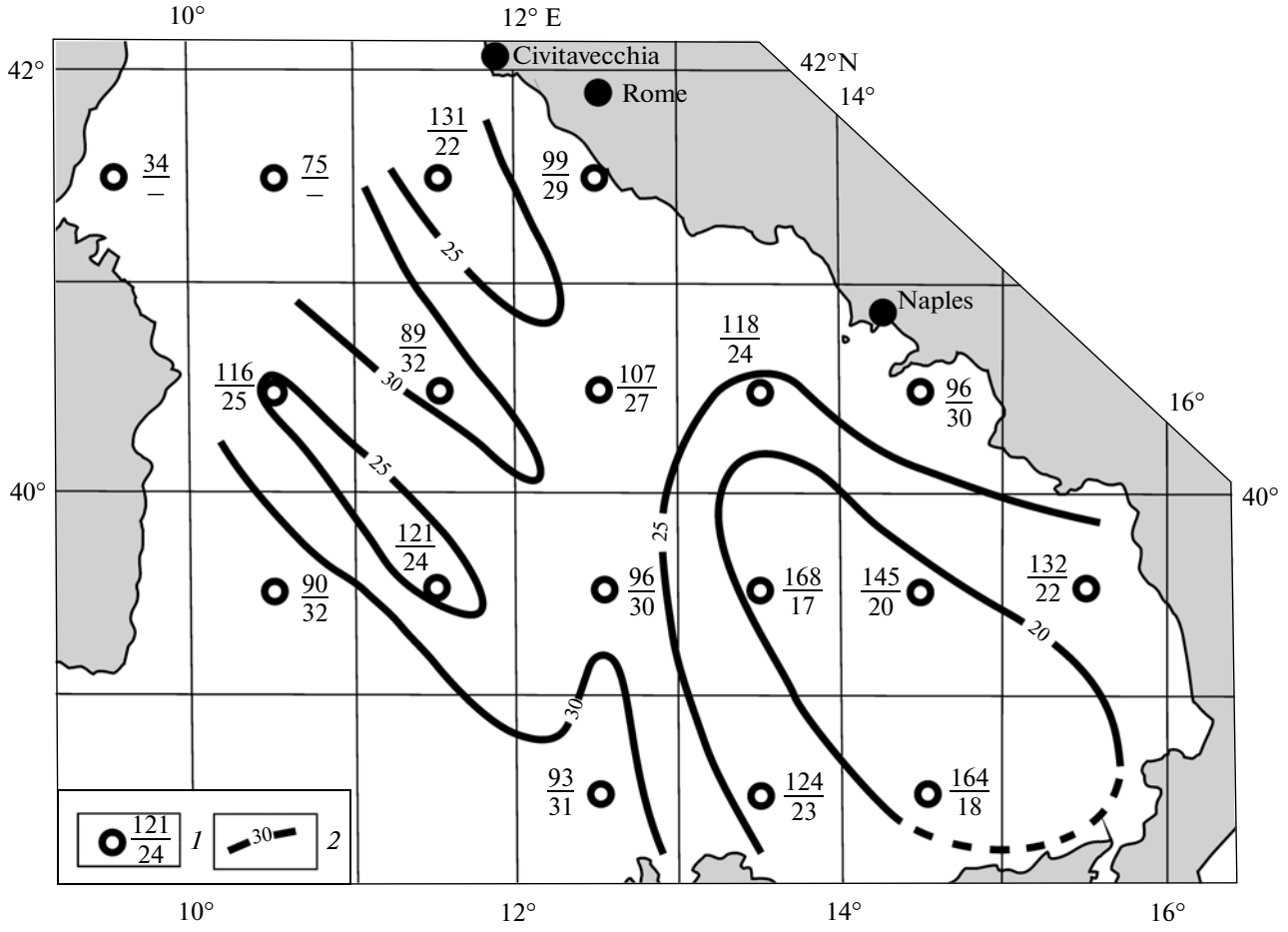

Fig. 3. Thickness of thermal lithosphere in Tyrrhenian Sea. (*1*) Nodal points: numerator, average heat flow, mW/m^2; denominator, lithosphere thickness, km; (*2*) contour line of lithosphere thickness, km.

As seen from this table, the Ethiopian and Afar zones of the African–Arabian Rift Belt (AAB) are the most heated and also distinguished by the most vigorous recent volcanism. Its average productivity in the Ethiopian zone over the Pliocene and Quaternary is estimated at approximately 16×10^{-6} km^3/yr [37]. This value yields to the recent productivity of volcanism in the Reykjanes Ridge estimated at $(40–50) \times 10^{-6}$ km^3/yr [36, p. 141]. In the studied part of the Red Sea ABB segment, productivity is lower ($\sim 23 \times 10^{-6}$ km^3/yr) [36, p. 111]. It is apparently close to that in the Afar Depression, where the total volume of Cenozoic volcanic rocks is estimated at 345000 km^3 [79]. To the south, in the Kenyan ABB segment, the productivity (11.5×10^{-6} km^3/yr) [37] is somewhat lower than in Ethiopia; the heat flow is lower too. Its mean value coincides here with that established in the Baikal Rift Zone (BRZ), although the intensity of recent volcanic activity in the BRZ is much lower. The heat flow density decreases along the strike of the AAB toward its ends, becoming less than 60 mW/m^2 in the Suez segment and still lower ($\leq$50 mW/m^2) in the Levantine, Nyassa, and Tanganyika segments. The heat flow in the BRZ varies in the same way, falling to a minimum in the Muya–Chara Zone at its northeastern ending (Table 1).

In general, the heat flow in continental rifts is lower than in axial MOR valleys; the dispersion of the measured heat flow values is lower here as well. In contrast to MOR, the average heat flows in different segments of rifts are variable. It is noteworthy that this dispersion is spatially ordered: the average value of conductive heat flow diminishes along the strike toward end segments. The same is noted in the AAB and BRZ. In the latter case, the maximum of average heat flow (87 ± 6 mW/m^2) is reached in the South Baikal Basin as a center of rifting [23, p. 182].

It is especially remarkable that such ordered variability of heat flow correlated with a decrease in mantle component of helium isotopic composition in hydrothermal solutions in both BRZ and AAB [16, 38]. The variable helium isotopic composition in continental rifts is their second difference from MOR, where ^{3}He/^{4}He remains constant on average $(1.15 \pm 0.1) \times 10^{-5}$ over the entire extent of the ridge in both bottom basalts and discharging hydrothermal solu-

Table 1. Heat flow in continental epiplatform rift zones and within-rift structural elements, mW/m^2, after [23]

Rift zone	Measured or inferred (in parentheses) heat flow				
	average throughout the zone	average in major within-rift structural elements*			
		on shoulders of rift basins	in rift basin	on within-basin uplift	in fault and volcanic zones
Ethiopian and Afar	(>100)	(<75)	(75–150)	–	(>200)
Rhona (Liman grabens)	100 ± 8	84 ± 5	110 ± 27	–	>125–150
Upper Rhine Graben	83 ± 16	74 ± 8	115 ± 31	124 ± 31	>100–180
Kenyan (Gregory Graben)	74	39–57	84–105	–	>200
Baikal (L. Baikal)	74 ± 7	56 ± 8	76 ± 7	69 ± 7	140 ± 18
Hövsgöl (Khubsugul)–Tunka	69 ± 7	48 ± 9	84–90	–	>100
North Sea	68 ± 4	60 ± 6	79 ± 8	–	>80–100
Suez	<60	42–47	60–80	–	>80–175
Tanganyika	(~50)	(<30–40)	48 ± 20	104	>75–150
Nyassa	(~50)	<20–30	42 ± 16	97 ± 22	>75–120
Levantine	48 ± 7	33 ± 13	51 ± 7	–	70 ± 9
Muya–Chara	45 ± 10	52 ± 10	51 ± 15	–	>60–90
Cameroon	~40	38 ± 2	42 ± 4	–	>60–80

* Accuracy of average estimate is shown as $\pm 1.96S/\sqrt{n}$, where S is dispersion and n is number of measurements.

tions [78], thus characterizing the ~~depleted~~ MORB reservoir. In continental hydrothermal solutions, the $^3He/^4He$ ratio in gases does not reach the MORB level except for the Afar plume, which removes helium from the undepleted mantle. The maximum values of this ratio mark centers of rifting similar to the South Baikal Basin in both the Afar segment of the AAB and in Rhine grabens [69].

The distribution of average heat flow and $^3He/^4He$ ratio in subsurface fluids sharply distinguishes continental rifts from MOR, despite the morphological similarity of rift basins and axial MOR valleys. Thus, the concept assuming different mechanisms of active rifting or spreading induced by invasion of mantle mass into the crust, on the one hand, and of passive rifting under the action of stresses external to the rift itself in continents [21, p. 13], on the other hand, is attested to by additional geophysical and geothermal argumentation. The passive rifting on continents results in the formation of pull-apart basins, the appearance of prerequisites for decompression melting of mantle matter beneath them, and emplacement of mantle-derived melt into the crust.

The constant He isotopic composition along the strike of MOR is considered evidence for a similar source of discharging mantle melts over the entire extent of MOR. On the contrary, the coherent variability of the $^3He/^4He$ ratio and heat flow in continental rifts indicates contamination of these melts with ^4He-enriched crustal matter. Such contamination is variable in degree depending on the extent of the rift opening along the strike or on the intensity of mantle diapirism [13]. Thus, the geophysical (geothermal) and geochemical (He isotopes) empirical approaches taken together support alternative models of rifting proposed in [21, 38, 58, 83]; they allow us to state that mantle activity during continental rifting is a consequence of deformation in the overlying lithosphere rather than a cause of this process. The deformation can be increased by ~~wedging action~~ of the ~~mantle~~ plumes ascending from the undepleted mantle if projection of plumes on the Earth's surface coincides with the rift zone, since the productivity of volcanism and intrusive magmatism at those sites is much higher than elsewhere [37, 38]. Judging by the He isotopic composition of fluids in the AAB, this took place in the Afar area and induced opening of the Red Sea.

Pericontinental rift zones. Specific geothermal anomalies occur at certain sites of passive continental margins, in particular, at the Svalbard ~~margin~~. This follows from heat flow measurements in the ~~Orla~~ (Storoya) Trench, which extends from the Kong Karls Archipelago in the south to the continental slope of the Nansen Basin in the north (Fig. 4). In this trench and at its extension on the continental slope, 28 heat flow measurements were carried out on board the R/V *Akademik Nikolay Strakhov* and yielded surprising results: 300–520 mW/m^2 [56]. This range is almost ten times higher than the background heat flow through the bottom of the Barents Sea and comparable with heat flow measurements in axial MOR zones.

The extrapolation of the temperatures derived from these data to the lower half-space shows that the supersolidus temperature can be encountered at a depth of 6.5–7.0 km under the trench bottom (Fig. 5). Such geothermal specificity of the trench in combination with its morphology shows that this structural element has a tectonic nature. It seems that this is a rift that crosscuts the Earth's crust for its total thickness and currently remains in active phase of development.

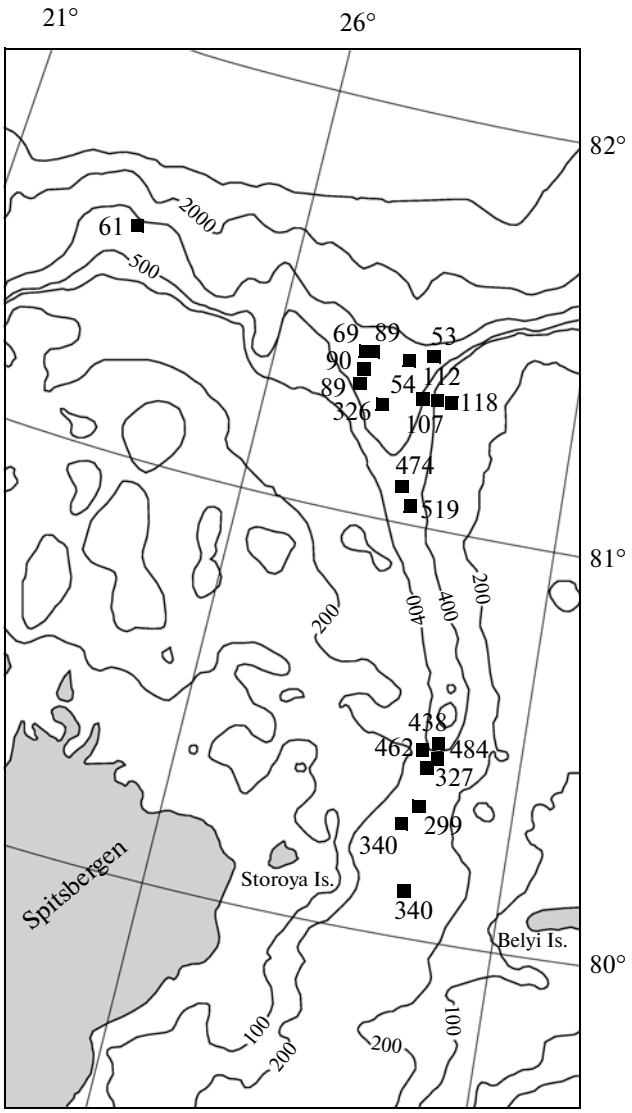

Fig. 4. Heat flow in ~~Orla~~ (Storoya) Trough. Heat flow values are given mW/m^2. Isobaths of 100, 200, 400, 500, 1000, 2000, and 3000 m are shown.

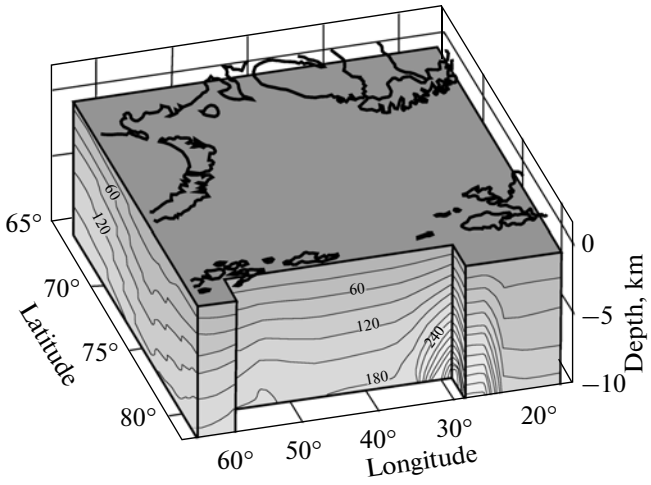

Fig. 5. 3D geotemperature model of Earth's crust in Barents Sea (view from north).

The ~~Orla~~ Trough is one in a system of troughs expressed in the bottom topography at the northern margin of the Barents shelf (Voronin, Svyataya Anna, Franz–Victoria troughs, etc.), which have been called grabens or rifts in recent years [4, 22, 27]. All of them are nearly parallel to the submarine Knipovich Ridge genetically related to the opening of the Atlantic Ocean. This suggests geodynamic ~~kindred~~ of oceanic and pericontinental rift zones, which explain similar heat flow in the ~~Orla~~ Trench, on the one hand, and in MOR and TFZ, on the other.

The high geothermal activity at certain sites of the Svalbard Plate is corroborated by Neogene–Quaternary volcanism in the Spitsbergen Archipelago [18] and by Iotun and Troll ~~gas-cut~~ springs heated to 26°C. The released gas phase contains up to 96% nitrogen [18]. The $^3He/^4He = (39–64) \times 10^{-8}$ of accompanying helium (oral communication by E.M. Prasolov) indicates an admixture of mantle component. In He isotopic composition, this gas is similar to that from springs in the Kolyuchino–Mechigmen rift in the eastern Chukchi Peninsula [42]. This similarity assumes to a certain degree identical geodynamic settings in these ~~distant~~ areas of the Russian Arctic ~~Region~~.

The localization of volcanic and hydrothermal activity of Spitsbergen along near-meridional faults and ~~westward~~ enrichment of volcanic rocks in alkali ~~metals~~ are considered as a consequence of ~~broader~~ opening of the Norwegian–Greenland Basin and Arctic Ocean [18]. Indications of submarine volcanoes are known to the north of Spitsbergen and high values of heat flow (110–125 mW/m^2) have been measured at the Yermak Plateau. All these data are consonant with hydrothermal activity along near-meridional dislocations at the margin of the Svalbard Plate.

PALEOZOIC FOLDBELTS

Beyond the zones of recent rifting, the geothermal field~~s~~ are quite distinct. The deep temperature and density of conductive heat flow are much lower; the intensity of heat efflux by means of magmatic and hydrothermal activity and corresponding general loss of heat drop sharply. Thousands of heat flow measurements in foldbelts on land make it possible to characterize the geothermal regime of any lithotectonic zones of the continental crust irrespective of their age.

In this section we focus our attention on ~~thermal fields~~ in zones of Paleozoic folding exemplified in the Central Asian Foldbelt characterized by numerous heat flow measurements, which are the basis for the complete and representative pattern of the geothermal field.

The vast Central Asian Foldbelt extends from the Pai-Khoi in the north to the Tien Shan in the south and from the Mugodzhary Mountains in the west to the Khingan in the east. This foldbelt is a combination of linear and mosaic fold zones. Having outlined them for the first time, Peive et al. [33] noted not only a difference in their geometry but also a number of distingushing geological and geophysical attributes, for example, distinct types of folding: holomorphic in linear zones and idiomorphic in mosaic zones; ~~HT–LP~~ metamorphism in former zones and HT metamorphism in the latter zones; metallogenic specificity with the predominance of chalco- and siderophile elements in linear zones and litho- and chalcophile elements in mosaic zones; different shapes of gravity anomalies corresponding to the geometry of fold zones. The main difference is expressed in the geodynamic mechanisms of continental crust formation. The allochthonous mechanism of crust transformation dominant in linear zones is expressed in lithotectonic rearrangements with the formation of subduction and collision zones as analogs of recent island-arc systems. The autochthonous mechanism of crust transformation is predominant in mosaic zones. Thrust–nappe structural elements are formed as well, but they have a smaller thickness, are not persistent along the strike, and, as a rule, have various ages in contrast to the linear zones, where the coeval nappes extend for a great distance [35, 46]. The autochthonous mechanism of transformation is primarily caused by compositional rearrangement of the crust by means of mantle material differentiation in the course of vertical heat and mass transfer. The Central Asian Foldbelt comprises tectonotypes of linear and mosaic zones. These are the Ural Foldbelt, including the Mugodzhary Mountains and the Central Kazakhstan Fold Region, respectively. The basically different heat flow distributions in these zones represent the main feature of the geothermal field in the Central Asian Foldbelt. Let us compare their thermal regimes.

The main geothermal feature of ~~the Ural Foldbelt~~ is the anomalously low heat flow density (20–35 mW/m^2), which is much lower than the global average for structural units of the same age (48–55 mW/m^2) [47, 50]. The anomalously low heat flow in Paleozoic linear fold zones is a global feature. The same as in the Urals, low heat ~~flows are~~ characteristic of the Appalachians [82], Salair [17], and South Mongolia [51]. The decrease in heat flow of linear foldbelts is related to their aforementioned geodynamic ~~formation~~ setting and evolution of the Earth's crust, which caused widespread thrust–nappe structure.

The quantitative models of the ~~heat~~ field evolution in allochthonous sheets (thrust models) were first considered in [50]. The situation when the geothermal gradient is negative naturally is not stationary, because the Earth's interior is heated to a higher temperature than the surface. A situation with a negative geothermal gradient can arise when thrusting develops. This situation gradually relaxes until the thermal structure reach a quasistationary state. Calculation has shown that the thermal regime disturbed by tectonic displacements in the over- and underlying sheets is recovered very slowly. When the thickness of an allochthonous scheet is 1 km, the heat flow reaches the stationary state in 5 Ma with an accuracy of 5%. If the whole lithosphere participates in thrusting, e.g., by the transformation of oceanic crust into continental, then the relaxation time stretches for hundreds of millions of years (Fig. 6).

The model in this figure is an alternation of the layers, and each layer has a specified thermal conductivity and radiogenic heat generation. The values of these parameters have been chosen from average statistical data characterizing the properties of the continental and transitional crust. The onset of solution ($t = 0$) corresponds to the moment when the bedding-plane thrust structure has arisen. It is suggested that the entire paleooceanic lithosphere 60 km in thickness participated in the formation of this structure.

At the moment $t = 0$, the temperature gradient at that depth was negative because of fast thrusting of the lithospheric sheet heated up to a temperature of 1200°C at its base over another sheet with a temperature of 0°C at its roof (Fig. 6). It has been accepted that the thickness of the layer with the negative temperature gradient is 10 km.

At the base of the lower sheet, the heat flow is assumed to be constant: 20 mW/m^2 at a depth of 60 + 60 +10 = 130 km. Such a mantle heat flow is established in recent convergent zones of western Pacific. The temperature of 150°C rather than 0°C was set at the roof of the lower sheet (point H) due to release of friction heat.

The sole of the upper block cools down with time, whereas the roof of the lower block heats up. Approximately 25 Ma after thrust formation, the negative temperature gradient in the fault zone disappeared, and 75 Ma later, a quasistationary temperature was established there; in 325 Ma, a quasistationary temperature distribution will be established throughout the lithosphere. The heat flow through the Earth's surface will decrease by approximately two times. In 225–275 Ma after thrusting, it will drop to the minimum and in 325 Ma it will increase and become, like the temperature field, quaistationary but two times lower than in the prearrangement period.

Thus, the thrust systems are characterized by decline of heat flow and then growth out to an asymptote that marks the onset of the quasistationary state. These two moments are distinguishing points of the thermal thrusting model. The time of arrival depends on the total thickness of the allochthon. The larger the thickness, the longer the time interval before a stationary point is reached and between the minimum and the moment of achieving a stationary regime [50].

The thrusting models also explain the growth of the geothermal gradient with approaching ~~of~~ the autochthonous block empirically established, for example, in SG-4 Superdeep drilled in the Tagil Synclinorium of the Central Urals [72].

The Central Kazakhstan Fold Region differs from the linear Ural Foldbelt in the mechanism of transformation of the Earth's crust and the character of the ~~thermal~~ field. In the opinion of Peive and his followers [19, 25, 26, 34], the autochthonous mechanism of crust transformation dominated in such mosaic (isometric) fold regions. The compositional rearrangement of the crust was related to differentiation of the ascending mantle material and lasted longer with a gradual buildup of a granitic–metamorphic layer from the margin to the center of the belt. An alternative concept of formation of the Central Kazakhstan Fold Region denies its mosaic structure and reproduces the present-day structural pattern as an arcuate turn of the initial island-arc structure [15]. Geothermal measurements disagree with this tectonic model.

The inward rejuvenation of the elements ~~pertaining to~~ the granitic–metamorphic layer correlates with the increase in the background (deep) heat flow. For example, the heat flow density in the Kokshetau (Kokchetau) Anticlinorium is 35 mW/m^2 (σ = 8); 39 mW/m^2 (σ = 4) in the Selety Synclinorum; 40–44 mW/m^2 in the east of the Uspensky Zone near its junction with Caledonides of the Shyngyz (Chingiz) Anticlinorium; 67–69 mW/m^2 at boundary of the Zhaman-Sarysu Anticlinorium and the Tokrau Basin; and 70 mW/m^2 (σ = 5) in the central part of the Tokrau Basin at the Aqshatau (Akchatau) deposit. Moving away from the Tokrau Basin to the west toward the West Balqash (Balkhash) Synclinorium and Zhezqazghan (Dzhezkazgan) Basin on the Caledonian basement, the heat flow somewhat decreases to 55 mW/m^2 [51]. The heat flow distribution in the Central Kazakhstan Fold Region is a regional example of global heat flow–age dependence in the continental crust [39].

Heat flow variation versus the age of tectonomagmatic activity producing volcanic–plutonic rock associations in mosaic fold zones can be explained by cooling of a mantle diapir (asthenolith) that intruded into the continental lithosphere. This process is described by the following model.

Let us assume that at moment $\tau = 0$, the roof of the asthenolith stopped at a depth of ~20 km, which corresponds to the location of the upper asthenosphere boundary in recent zones of scattered spreading (see above data on the Tyrrhenian Sea). At a greater depth, temperature increases downward with an adiabatic gradient. The calculated change of temperature and heat flow during the next billion years is shown in Fig. 7. The problem was solved under boundary condition of the second type (constant heat flow at the lower boundary at a depth of 350 km, which is more plausible in this model than a constant temperature). The

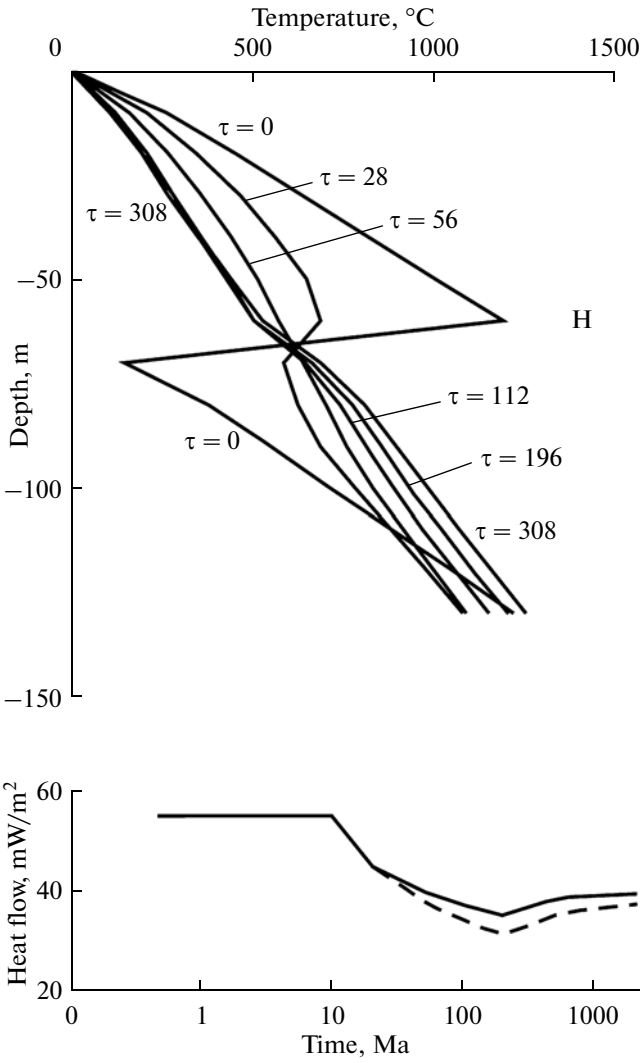

Fig. 6. Variation of geothermal field under conditions of thrusting at boundary conditions of type II at lower boundary. Time-dependent variation of temperature after formation of thrust fault at time τ is shown above. Time-dependent variation of heat flow is shown below, with (solid line) and without (dashed line) allowance for release of phase transition heat.

invariant heat flow from the mantle at that depth during ~10^9 yr is only an arbitrary assumption, since heat flow actually decreases due to exhaustion of its sources.

The simulation has shown that the matter crystallized and cooled with time in the upper part of the lithosphere at a depth of ~200 km. The temperature grows with depth, but slowly because of a low adiabatic gradient. In 50 Ma, temperature at a depth of 350 km rises by 200°C and by 250°C in 100 Ma. The rate of the temperature increment decreases with time. A zone with an adiabatic temperature gradient continues to exist at intermediate depths. At time moment τ = 10 Ma, this zone is located within a depth interval of 80–240 km; at τ = 50 and 80 Ma, those depth intervals are

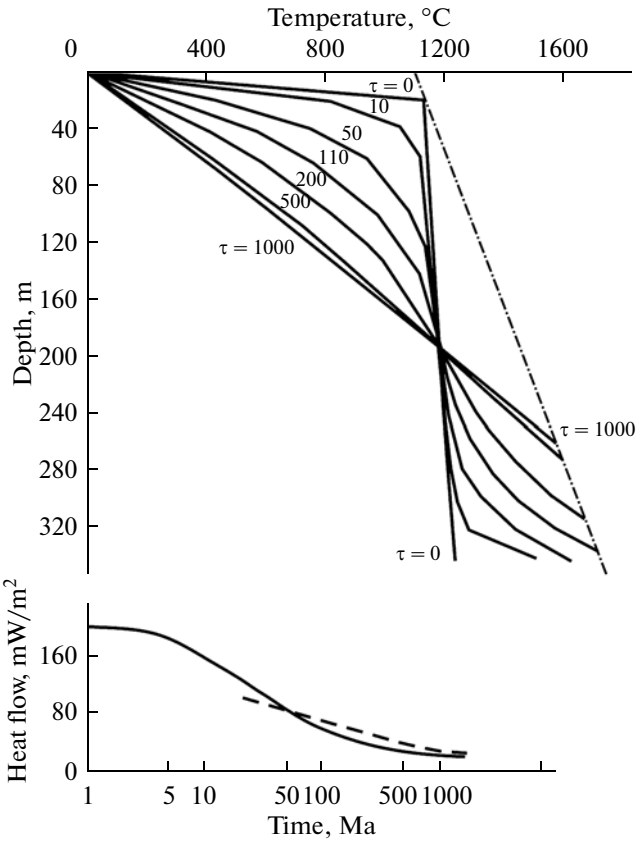

Fig. 7. Thermal field evolution under conditions of cooling and crystallization of matter under type II boundary conditions at lower boundary. Variation of temperature in lithosphere shown above; variation of heat flow at surface of given model (1) and in empirical relationship (2) after [39] shown below. Dashed line indicates geotherm of basalt solidus.

160–220 and 180–210 km. These zones probably correspond to asthenolenses, or astenosheets in the terminology used in [32], localized within the more viscous lithosphere.

In 50 Ma after onset of the process, the geothermogram crosses the solidus curve of mantle material at a depth of ~360 km. Since this time, fractional melting has proceeded at a higher temperature corresponding to the thermodynamic setting at the migrating upper boundary of the asthenosphere. Afterward, the boundary of fractional melting will move upward. Thermal energy will be absorbed as a result of the phase transition with a decrease in heat flow. Note, however, that the equivalent heat flow density of phase transition is lower than the deep heat flow by approximately an order of magnitude [14].

The quasi-stationary state of temperature distribution is achieved in 10^9 yr, when the depth of frational melting reaches 250–260 km. The thickness of the lithosphere in Central Kazakhstan is estimated at the same value on the basis of magnetotelluric evidence [1].

The variation of heat flow at the Earth's surface calculated from this model is akin to the variation of heat flow in the continental crust depending on the age of the last stage of tectonomagmatic reactivation (Fig. 7~~b~~).

Thus, the model of cooling and crystallization of the asthenosphere satisfies the observed geothermal field in mosaic fold zones and explains the relationship between heat flow and the age of magmatic activity. Deviations from this relationship are caused by perturbation of the geothermal field by tectonic movements (see above) or by other factors, including radiogenic heat generation in rocks.

As is known, radiogenic heat is released during the decay of ^{238}U, ^{235}U, ^{232}Th, and ^{40}K. This effect is higher in felsic rocks; in basalts and ultramafic rocks, it is 12–15 times lower. If the average surface heat generation (2 ~~mW/m^2~~) is ascribed to the upper 30–40 km of the continental section, then this process would provide all conductive heat losses established in the continental block. Nevertheless, the heat flow from the mantle as the second component of heat flow measured at the surface cannot be zero or, moreover, negative. In addition, no universal correlation exists between the heat flow density and thickness of the crust. These constraints spurred us to develop thermal models of the lithosphere, which assume a decrease in heat generation with depth [61, 73, 82].

Both heat flow components are subdivided on the basis of linear relationship between their values in the drilled depth interval and heat generation:

$$q_s = q_m + DA_s,$$

where q_s and q_m are heat flows measured at the surface (s) and supplied from the mantle (m) to the sole of the heat-generating layer (crust); A, surface heat generation; and D, the linear regression factor, which is equal to the depth of the active heat-generating layer [61].

At least three models of radioactive element distribution fit the heat generation decreasing with depth: stepwise, linear, and exponential. The stepwise model is used where the crustal section is well-studied and makes it possible to impart specific heat generation value to each layer. The other two models are applicable to provinces, where the crustal section remains insufficiently studied, although available drill holes make it possible to establish a correlation between surface heat flow and heat generation.

The first model was applied to scrutinize the heat flow structure in the southern Urals and central Kazakhstan, whereas the second and third models were for Mongolia, where the structure of the Earth's crust is insufficiently clear.

Using the published data, the following A values (~~mW/m^2~~) have been accepted for the southern Urals and central Kazakhstan: the granite–metamorphic layer: 1.55 (2.31 in the upper part and 1.26 in the lower part); the basaltic layer: 0.46 (0.67 in the upper part and 0.25 in the lower part); and the upper mantle: 0.008 [51].

Based on the accepted A_s and D values, thermometric data on boreholes, and the crustal structure [6], lateral variations in q_s measured ~~at~~ the surface, radiogenic (crustal) heat flow (q_r), and mantle heat flow (q_m) have been ascertained. The latter heat flow, which is often called reduced, was calculated as the difference $q_m = q_s - DA_s$. These variations are demonstrated in Fig. 8. The shown sections are based on the results of thorough thermal studies at a number of deposits. In each of them, heat flow was measured in several holes and its radiogenic (crustal) component was determined from core samples. In the Central Kazakhstan Fold Region (from Tobol to Balqash (Fig. 8)), this component is independent of the age of the tectonic unit ~~(Fig. 8)~~, which correlates with both surface and mantle heat flows. In central Kazakhstan, the latter increases with rejuvenation of the Earth's crust from 15 mW/m^2 for Late Riphean age to 32 mW/m^2 for Middle Carboniferous; the surface heat flow increases from 35 to 70 mW/m^2. Thus, the crustal radiogenic component amounts to 40–50% of the observed value for most objects. Only in the Tokrau Basin (Aqshetau site) ~~does~~ the radiogenic heat flow (45 mW/m^2) ~~reach~~ 60% of the background value (74 mW/m^2) owing to the high concentration of lithophile chemical elements in the Aqshetau granitic pluton [5], along which U and Th are removed into the upper crust [71].

Using the exponential model, we processed the geothermal data on Mongolia [51]. In the total selection of 45 pairs q_s and A_s values, the surface heat flow varies from 16 to 75 mW/m^2, and surface heat generation, from 0.55 to 3.16 μW/m^3. The mantle heat flow is estimated at 23 mW/m^2. This ~~section~~ is, however, inhomogeneous because the Mongolian territory consists of the North Mongolian Mosaic Megablock and the linear South Mongolian Hercynian Foldbelt similar to the Ural Foldbelt [19]. In the South Mongolian Foldbelt, nine pairs of q_s and A_s values yield a surface heat flow varying from 16 to 40 mW/m^2 and surface heat generation from 0.55 to 3.16 μW/m^3. The mantle heat flow is estimated at 14 mW/m^2. The low q_s and A_s values in the South Mongolian Foldbelt, like in the Ural Foldbelt, are a consequence of the predominantly allochthonous mechanism of its formation [51].

In summary, the contribution of radiogenic heat to the average values of the observed heat flow in both the mosaic North Mongolian geoblock and linear South Mongolian Foldbelt is estimated at 40–50%.

SEDIMENTARY ~~BASIN~~

In contrast to foldbelts, which make up a cratonized portion of the Earth's crust, sedimentary basins form its cover. Together with the overall similarity of these zones accumulating relatively loose materials, vast platform sedimentary basins are distinguished from relatively narrow orogenic and taphrogenic troughs by (a) morphology and size; (b) age of basal units, i.e., duration of sedimentation; and (c) geodynamic settings of their origin and evolution with subdivision into loading and extension basins according to helium isotopic composition [80]. These distinguishing features are emphasized by contrasting geothermal attributes.

Over the last 20–30 years, the geological and geophysical study of sedimentary basins has been the main focus of geologists [28]. This is due to the importance of this research for solving general problems of the formation and evolution of the Earth's crust and the significance for forecasting and prospecting mineral deposits, especially hydrocarbons. In this connection, study of the thermal regime in a sedimentary basin has seen substantial progress [8–10, 12, 20, 29, 52, 55, 57, 63].

The use of 3D geothermal modeling (thermal tomography technique [55]) has demonstrated the possibility of revealing temperature and heat-flow anomalies, which cannot be established from a 1D and 2D distribution of these parameters. The higher informational capability of 3D geothermal models is especially evident for isometric basins. Thermal tomography makes it possible to specify the position of temperature boundaries, which control the generation or transformation of materials, e.g., catagenesis of organic matter, facies of regional metamorphism, and depth of the Curie isotherm, i.e., a tool to correctly visualize factual geothermal data and reliably interpret them.

The thermotomographic modeling technique is described in [53, 55, 57]. In particular, these publications show the links of temperature anomalies to ~~subsurface~~ petroleum resource potential in many land and shelf provinces and propose the notion of a thermal dome, emphasizing the localization of hydrocarbon accumulations in zones of ascending geotherms. The physical sense of thermal domes is related to the mutual influence of beds varying in thermal conductivity and their deviation from a flat parallel attitude in the sedimentary cover. Therefore, the lateral temperature distribution reflects the localization of structural traps.

Let us consider three examples of thermotomographic modeling of the Pericaspian ~~Basin~~, the West Arctic shelf loading ~~basin~~, and the Pannonian extension basin. The geology and evolution of these basins have been described in [29, 30, 76].

In the *Pericaspian Basin*, the ~~thermal~~ field has been represented based on the temperature distribution in holes ~~recovered~~ after drilling, measurements of the thermal conductivity of the penetrated rocks, and seismic reflection CDP profiling results, which ascertain the crust structure.

The temperature distribution in section of the Pericaspian Basin has been established by 3D interpolation of the factual data from irregular network tied up to the drill hole coordinates and the strike of seismic

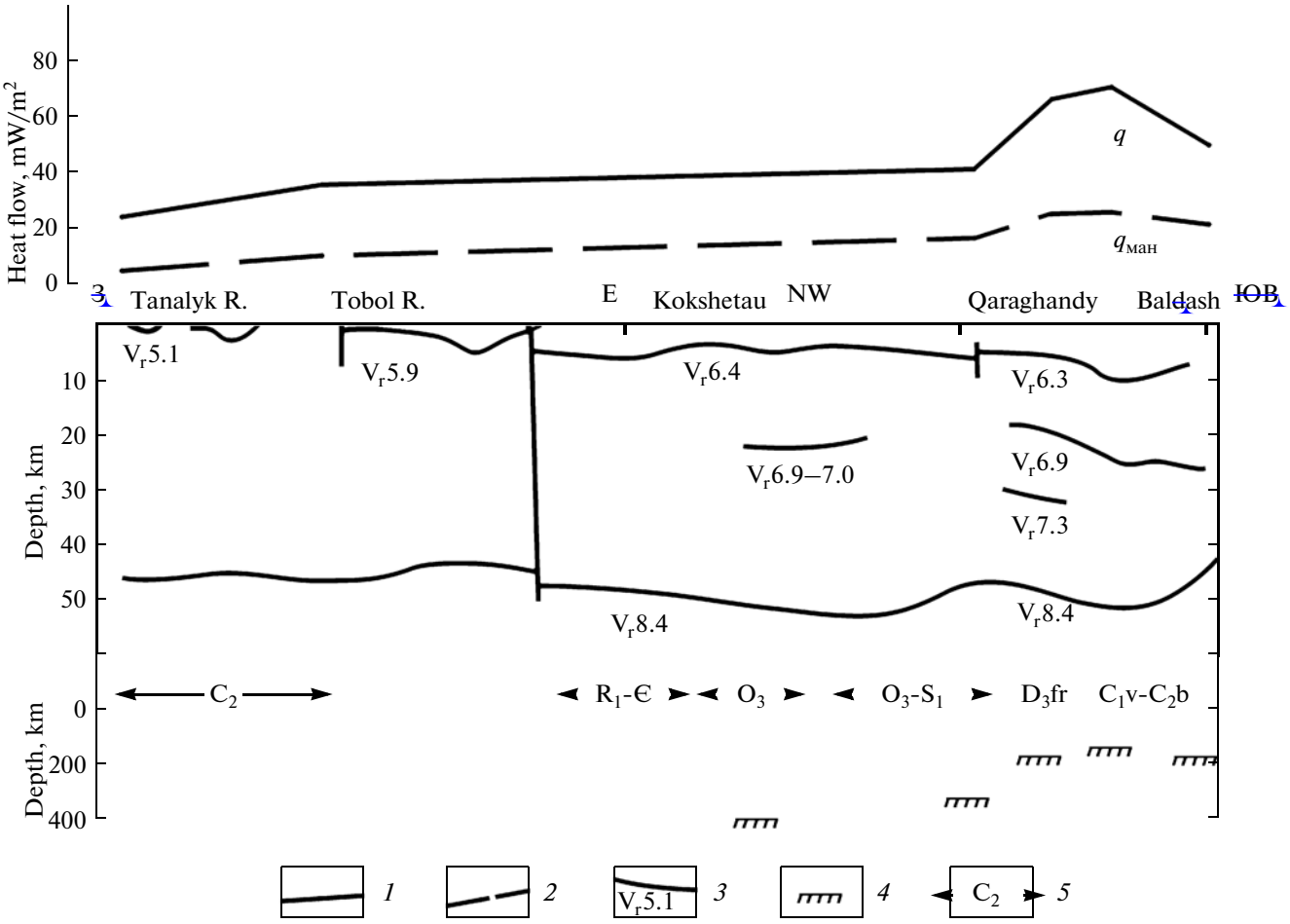

Fig. 8. South Ural–Balqash geothermal section. (*1, 2*) Heat flow: (*1*) through Earth's surface, (*2*) through Moho surface; (*3*) seismic boundary and boundary velocity (km/s) from DSS data; (*4*) upper boundary of asthenosphere calculated from geothermal data; (*5*) time of granite–metamorphic layer formation, after [25].

lines (Fig. 9) used for 2D calculation of deep temperatures.

As is shown in Fig 9b, the deep temperature rises in depth interval 0–5 km from northeast to southwest. In eastern part of the basin, the temperature at depths of 2 and 3 km are 40–45 and 60–65°C, respectively, whereas in the South Emba district and Manggyshlaq (Mangyshlak) Peninsula, the temperatures at the same depths are 55–60 and 70–75°C. This indicates that the heat flow diminishes in the east due to screening of the deep heat flow in the southern Urals and Mugodzhary Mountains in the geological past (see above).

A similar model has been created for depth interval of 0–50 km including the entire crust of the basin as a whole (Fig. 9c). The seismic wave velocities along profiles have been used for this purpose [7, 28, 31, 48]. The deep temperatures have been calculated along the seismic lines by means of numerical simulation [52]. Comparison of calculated and empirical data from drill holes shows their perfect convergence: a discrepancy is only ±50 m at a depth above 5 km and ±150 m down a depth of 40 km, i.e., a relative uncertainty of approximation does not exceed 1%.

As in the drilled depth interval, the temperature also smoothly increases to the southwest in a depth interval of 0–50 km (Fig. 9c). In the east of basin, the temperature at the Moho discontinuity is 400°C and coincides with that calculated beneath the southern Urals and Mugodzhary Mountains [51], but in the central and especially South Emba parts, the temperature is somewhat higher, reaching 450–500°C. Ascending westward from the longitude of the Mugodzhary Mountains, the isotherms form several domes, the apices of which are localized in the areas of South Emba, Mertvy Kultuk Sor, the North Mangghyshlaq (Mangyshlak) Peninsula, as well as in the Astrakhan and Buzuluk arches [57]. Thus, the spatial association of thermal domes and zones with economic petroleum resources occurs in the Pericaspian region as elsewhere.

In the *West Arctic Region*, the geothermal field is inhomogeneous. The most contrasting geothermal gradients are established in the east and southeast of

the Barents Sea and in the South Kara Basin. The background temperatures at depths of 3 and 5 km are 90–100 and 125–140°C, respectively. The positive temperature anomalies with amplitude rising with depth from 20 to 40°C are noted locally. In 3D distribution of deep temperatures, the rise of isothermal surfaces in the southeastern and eastern parts of the Barents Sea, including those, which control interval of organic matter catagenesis, forms a dome, where petroliferous fields are localized (Fig. 10; Table 2).

The accuracy of calculated thermotomographic 3D models was estimated by coincidence of simulated heat flow and measured in drill holes or/and by coincidence of temperature at intersections of seismic lines. The absolute uncertainty in isotherm location at such intersections with estimated with the least square technique is ±150 m (relative uncertainty at a depth of 30 km is 0.5%).

The Pannonian Basin in Hungary, which has been comprehensively studied by geological, geophysical, and geochemical methods [29, 84], arose owing to extension of the lithosphere, which started 19 Ma ago and resulted in the rise of the asthenosphere, thinning of the crust down to 25–50 km, and compensating accumulation of Mio- and Pliocene volcanic–sedimentary sequences up to 7 km thick (seismic reflection CDP evidence). Volcanic activity is a pictorial result of discharge of thermal and mass deep-seated flows into the basin, which is supported by geothermal evidence integrated by Lenkey [1999].

According to these data, the temperature in the Pannonian Basin reaches 200°C at a depth of 5 km and the average heat flow is 101 ± 6 mW/m^2 with local maximums up to 130–140 mW/m^2 (Fig. 11). The NE-trending zone of anomalously high heat flow extends to the Transcarpathian Basin of Ukraine. At such high parameters of the geothermal field, the geotherm of the basalt solidus can be reached at a depth of 40–50 km. Thus, the Pannonian Basin is a structural unit with an anomalously thin crust and lithosphere thermally activated in the Miocene to Pliocene. The decreased viscosity of the hot lithosphere facilitates relaxation of elastic stresses. This can explain the relatively low seismicity of the Pannonian Basin, where only sporadic seismic events of $M = 4$ have been recorded.

To calculate the deep temperature in the lithosphere of the Pannonian Basin and the adjacent territory, we carried out 2D modeling of deep temperatures and heat flow along the network of seismic lines (Fig. 11) shot in 1980–2004 by specialits from Ukraine, Austria, the Czech Republic, Poland, and Hungary [76].

The 3D model created with volumetric interpolation of 2D sections (Fig. 12) revealed a zone of thinned lithosphere beneath the Pannonian Basin. As is seen from Fig. 12, the forecasted projection of the supersolidus temperature extends in the northeastern direction beneath the adjacent Transcarpathian Basin, where a local asthenolens is outlined. As judged from

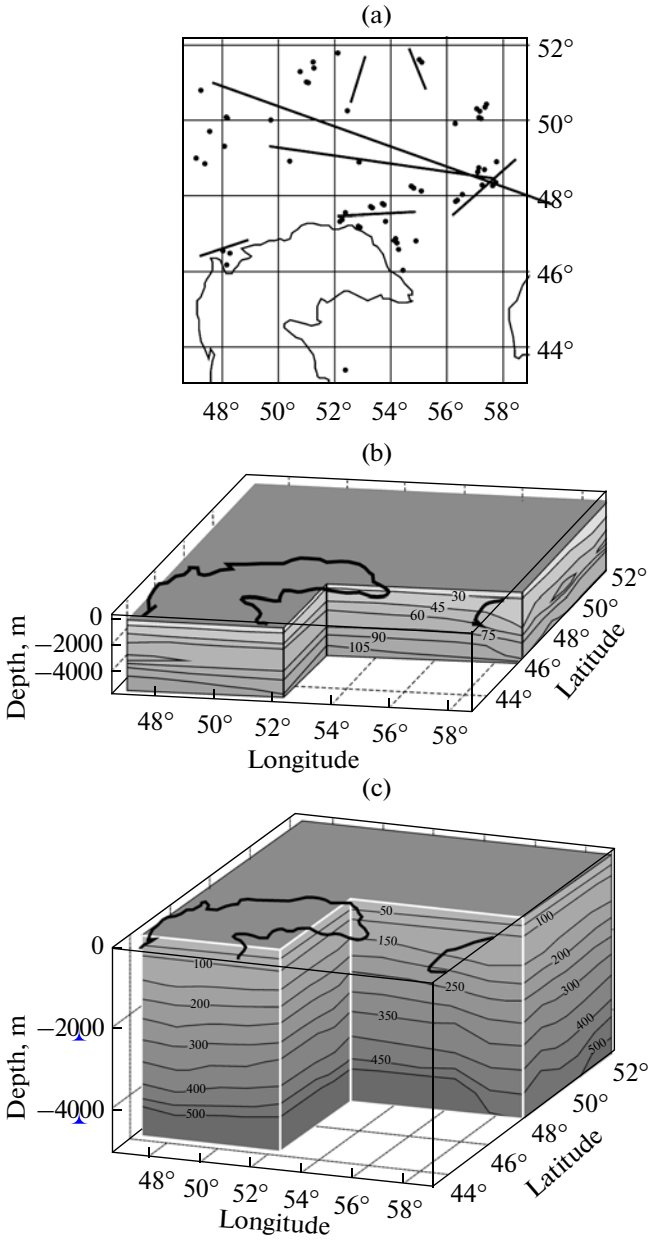

Fig. 9. 3D models of deep temperature distribution in Pericaspian Basin: (a) location of holes and seismic lines used for geothermal modeling; (b) temperature distribution within interval of drilling (0–5 km); (c) same in Earth's crust (0–50 km).

the shape of isotherms, the heated material penetrated into the basement of Transcarpathian Basin in the lateral rather than vertical direction from the side of the Pannonian Basin after formation of the asthenospheric jut, i.e., in the late Miocene. The thermal activation of both structural units standing out against the relatively quiet background of the central Europe is expressed not only in the high conductive heat flow but also in outlets of thermal springs and Late Cenozoic volcanic activity.

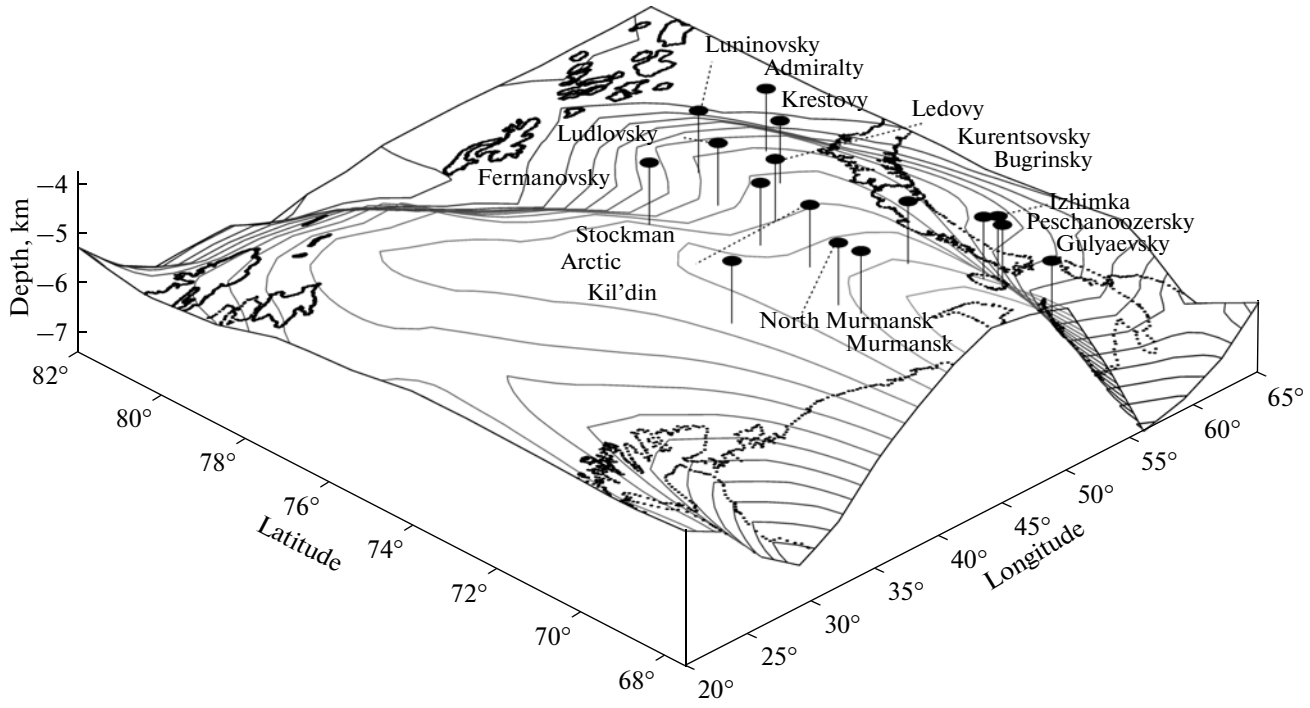

Fig. 10. Isothermal 140°C surface and localization of holes in hydrocarbon fields (filled circles) in eastern part of the Barents Sea related to thermal dome.

This hot spot of Europe, as Khorvath [49] once called the Pannonian Basin, stands out not only by physical manifestations of geothermal activity. Like in rift zones, these manifestations are accompanied by the appearance of mantle-derived helium in subsurface ~~aqueous~~ fluids. The highest $^3He/^4He$ ratio measured in thermal water from Pliocene felsic tuff of the Pannonian Basin reached 550×10^{-8} [66], and this value is only twice as low as the isotopic signature of the MORB reservoir. Almost the same values ($200–320) \times 10^{-8}$ were determined in springs heated to 55°C at the Vygorlat–Guta volcanic ridge. The occurrence of mantle-derived helium in the subsurface fluids of these and other identical depressions validates their definition as extension basins in contrast to foredeeps, foldbelts, and syneclises of ancient platforms [80]. In the greater part of the East European Platform, including the exogonal Timan–Pechora Basin and the Pericaspian Basin, poorly studied in this respect, as well as the Carpathian and Caucasus foredeeps, the helium isotope ratio in gases corresponds to the canonical radiogenic value inherent to the Earth's

Table 2. Heat flow density measured in deep drill holes in southeastern Barents Sea, after [20]

Hole, site, number	Coordinates		Measurement interval, m	Geothermal gradient, mK/m	Heat conductivity, W/(~~m K~~)	Heat flow density, mW/~~M~~^{2}
	north lat.	east long.				
Stockman, 1	73.0	44.0	2000–2150	30.0	2.43	71
			2722–3070	24.4	2.84	
Arctic, 1	71.7	43.6	2500–2570	31.4	2.43	77
			2640–2670	31.4	2.42	
			2845–2925	31.3	2.45	
Admiralty, 1	75.65	53.15	1050–2610	38.4	2.4	92
Krestovy, 1	74.5	50.46	1600–3000	29.1	2.4	70
North Kil'din, 82	71.58	37.1	2973–3098	35.2	2.39	84
Ludlovsky, 1	74.86	46.78	1305–1710	39.7	1.8	71
Murmansk, 26	69.9	41.7	2030–2530	30.8	2.2	68
Kurentsovsky, 1	70.45	47.2	210–380	36.4	1.6	58
Prirazlomny, 1	69.316	54.751	2429–2802	24.7	2.45	60

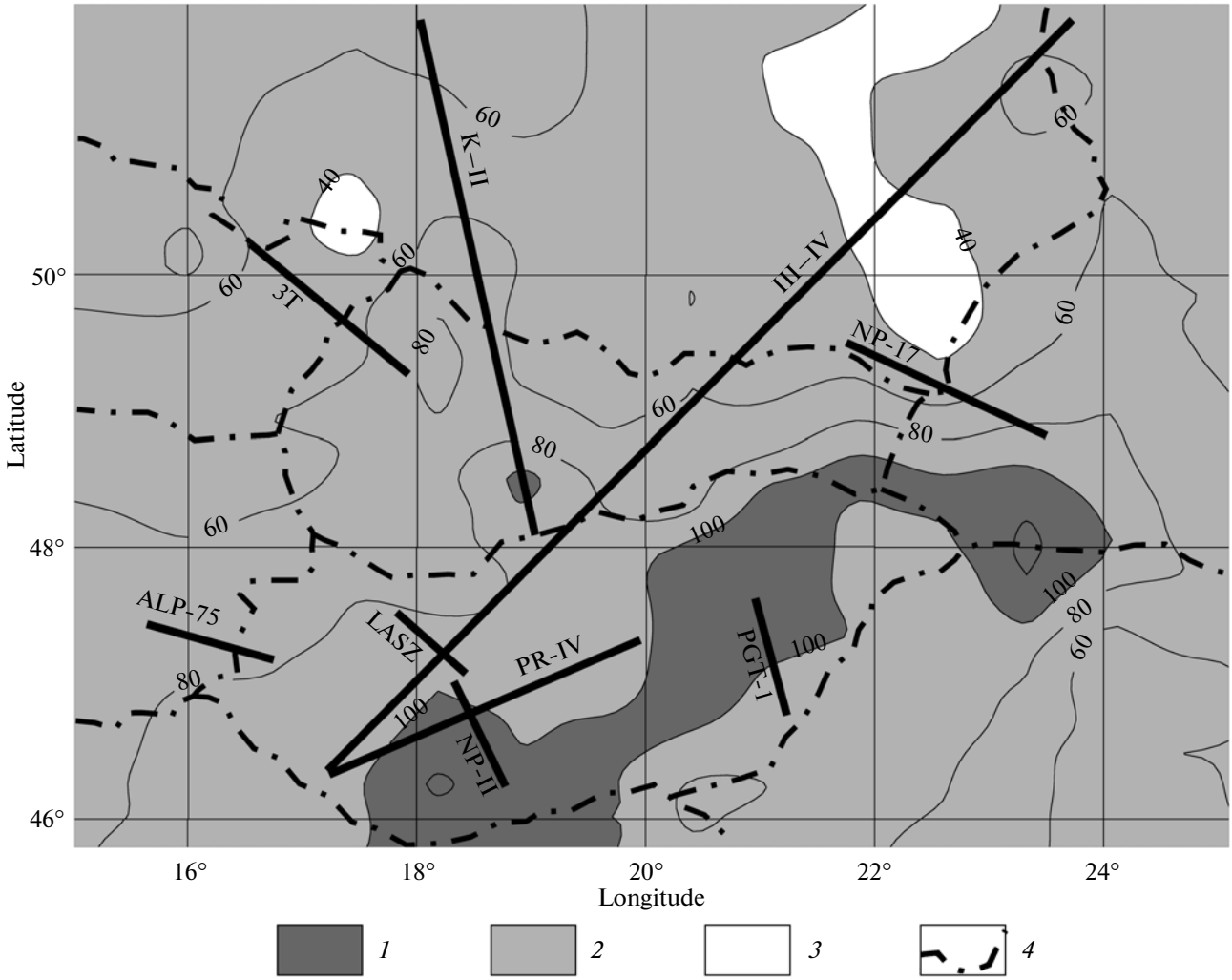

Fig. 11. Contour lines of heat flow in Central Europe and location of seismic lines used for geothermal modeling. (1–3) Zones of heat flow: (*1*) elevated, (*2*) background, (*3*) lowered; (*4*) state boundary.

crust ~$(2 \pm 1) \times 10^{-8}$ [24, 43]. Such helium is generated in the fill of these depressions related to loading basins [80].

The ages of the considered basins are appreciably different. In the Pericaspian and Barents–Kara regions, the main periods of ~~sagging~~ fall on the Middle and Late Paleozoic and Early Mesozoic, whereas in the Pannonian Basin a quarter of the total crustal thickness falls on the Miocene felsic volcanic rocks [29]. If the thermal regime of the considered loading basins is reconstructed issuing from the heat flow–age relationship, then heat flow density at the time of their origination (~300 Ma ago in Arctic Region and ~270 Ma in the Pericaspian Region) could have exceeded by no more than 20 mW/m^2 and anyway was twice as low as the currently observed heat flow density in the extension Pannonian Basin, which has in addition been significantly reduced by consumption of the deep heat flow by rapidly deposited sediments [77]. Thus, the main cause of sharply contrasting heat flows in basins of various types is related to the age and intensity of tectonothermal activity rather to the time of their origin. In the Pannonian Basin, this activity was expressed as a rise of the roof of the asthenosphere and anomalous heating of the overlying sequence of rocks. The history of the Pannonian Basin is close in this respect to the inferred history of the Tyrrhenian Sea as noted by Boccaletti et al. [~~1976~~]. A certain similarity of the geodynamic settings in the zones of scattered spreading and the extension sedimentary basins caused by the rise of mantle material can be apparently confirmed, although the evolutional trends of ~~either~~ structural units requires further investigations. The formation of loading basins is explained by other causes [2, 3].

Thus, the main conclusion from geothermal research of sedimentary basins should be focused on the appreciable difference in heat flow density in loading and extension basins. In the former basins, the heat flow in the cover depends on the age of the basement but is subject to the action of distorting factors prima-

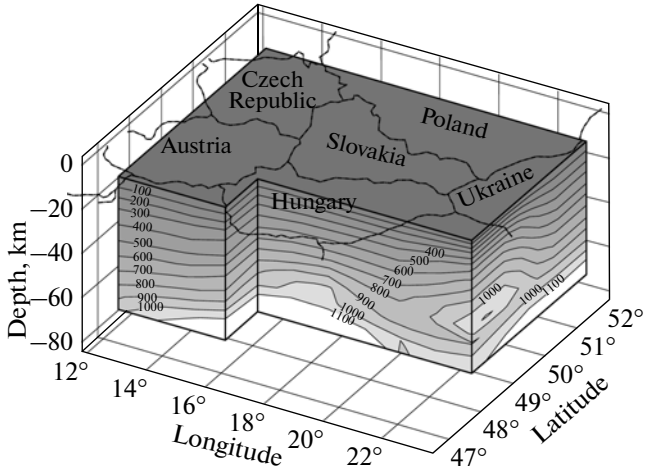

Fig. 12. 3D geothermal model of central Europe.

rily related to structural and thermophysical heterogeneities that formed under conditions of contrasting thermal conductivity and to the hydrodynamic factor. All this results in the appearance of local temperature anomalies in the sedimentary cover, which, as it turned out, coincide spatially with the localization of petroliferous provinces and fields. The heat flow is anomalously high in extension basins owing to reduced thickness of the lithosphere as compared with loading basins. The extension basins are probably structural elements corresponding to the initial stage of areal spreading zones.

CONCLUSIONS

The evidence presented in this paper attests to specific geothermal fields in various structural elements in the Earth's crust, ~~which differ in their~~ parameters, primarily, in heat flow density~~;~~ in spatial distribution~~;~~ and time-dependent evolution. The geodynamic settings of origin and development of certain structural units are reflected in these features. The studied structural units pertain to three major tectonic taxons: rift zones, foldbelts, and sedimentary basins, which represent zones of oceanic spreading and continental rifts, linear and mosaic foldbelts, and extension and loading basins. As was clarified, the considered taxons and their elements are characterized by contrasting geothermal features.

The rift zones are distinguished by the most intense geothermal activity in all its manifestations: volcanic activity, discharge of geothermal waters, and conductive heat flow density. The average (background) latter parameter in axial zones of MORs is higher than its global average value by five to six times, and particular values are higher by approximately 30 times, sharply decreasing to the flanks. The conductive heat flow density in centers of continental rifting is somewhat lower but remains of the same order of magnitude. In contrast to MORs, the conductive heat flow density in continental rifts decreases not only across their strike, but also along the strike from center of rifting toward both ends, as was shown by study of the Baikal Rift Zone. This ordered variability of heat flow correlates with the $^3He/^4He$ ratio decreasing from a maximum in the center of rifting, which is locally close to the mantle value ~~and~~ to the ratios close to crustal radiogenic helium at a distance from this center. This does not occur in MORs due to the same degree of opening ~~rather in contrast to a variable degree in~~ the Baikal Rift Zone and other continental rifts.

In Paleozoic foldbelts, the measured values of the background conductive flow density are much lower. In the mosaic belts they vary according to the well-known relationship of the average measured heat flow versus the age of tectonomagmatic activity, e.g., from 38 to 70 mW/m^2 in central Kazakhstan (the contribution of radiogenic heat is 40–50%). This activity is caused by the appearance of additional heat sources from time to time; a priori, these sources are related to mantle diapirs.

The time-dependent heat flow in the Phanerozoic fold zones clearly indicates the transient character of continental geothermal field in this period of geological history. The time-dependence is redoubled by the activity of factors that distort deep heat flow, especially as concerns tectonic movements. That is why the heat flow in linear foldbelts, in the Urals, Appalachians, etc., is much lower, dropping to 25–28 mW/m^2 because of long-term perturbations of the natural geothermal field by horizontal tectonic movements forming a thrust–nappe structure.

In the linear belt of the southern Urals, the mantle heat flow component is the lowest (8 mW/m^2, i.e., 25% of the background heat flow). Thus, the anomalously low heat flow in the Ural Foldbelt is caused by a decrease in both the crustal and mantle heat flow components.

Specific time-dependent thermal anomalies in sedimentary basins arise due to fast accumulation of "cold" sediments. Part of the deep heat flow is consumed for heating of these sediments to the background temperature. In loading basins, the mean conductive heat flow more or less corresponds to the age of the basement; however, the structural and thermophysical inhomogeneities of the sedimentary cover and water circulation can disturb the deep flow and create thermal domes promising for hydrocarbon accumulation, e.g., in the Pericaspian Basin or the ~~w~~estern Arctic region. In extension basins, the contemporary heat flow depends on the age and degree of tectonothermal activation of the lithosphere beneath these depressions. The activation of such basins is reflected in the enrichment of fluids circulating through the sedimentary cover in mantle-derived helium in contrast to ~~extension~~ basins. The similarity of deep settings in extension basins and zones of scattered spreading is recorded in the geothermal features.

The study of heat flow in various tectonic units allowed us to reveal the specificity of the ~~thermal~~ field in certain contrasting geodynamic settings. At the same time, certain unsolved problems became more distinct. They involve:

(1) spreading of comparative analysis over the entire range of crustal structural elements, primarily, on continents, using thermotomographic modeling of these elements and specifying proportions of crustal and mantle heat flows;

(2) unambigous mapping of lateral heat flow variations and elucidation of their links to tectonic regionalization of the continental crust (problem of averaging);

(3) estimation of the role of erosion not only as a factor changing the temperature at the upper boundary of the lithosphere, but also ~~controlling~~ the phenomena that remove heat-generating substances with the highest concentrations of radioactive elements from geological section;

(4) study and interpretation of asymmetric distribution of heat flow relative to axes of oceanic spreading and continental rift zones;

(5) more precise estimation of the thickness of the thermal lithosphere in various structural units, where this thickness is determined with independent methods (seismology, magnetotelluric sounding).

The solution of these problems is a necessary condition of realistic (physically plausible) geotectonic ~~developments~~ satisfying available geological information and eventually leading to the creation of a general model describing the formation and evolution of the Earth's crust.

ACKNOWLEDGMENTS

We thank M.P. Antipi~~n~~, V.R. Akhmedzyanov, Yu.A. Volozh, A.V. Ermakov, A.M. Gorodnitsky, A.Ya. ~~H~~olmstock, I.L. Kamensky, V.G. Levashkevich, Yu.G. Leonov, L.V. Podgornykh, E.M. Prasolov, V.N. Puchkov, I.N. Tolstikhin, and L.A. Tsybulya for their assistance in fieldworks, advice, and constructive criticism. Important information on the Pannonian Basin was kindly placed at our disposal by L. Lenkey from Eötvös Loránd University, Budapest, Hungary. With gratitude and sadness we remember the help of bygone colleagues: V.I. Kononov, V.E. Sal'nikov, and I.B. Dal'yan. This study was supported by the Russian Foundation for Basic Research (project no. 11-05-00047), Division of Earth Sciences, Russian Academy of Sciences (program "Interaction of Geospheres: Geophysical Fields and Mass Transfer"), and the federal target program "Human Resources in Science and Education for Innovative Russia~~."~~"

REFERENCES

1. D. Al'mukhanbetov, E. Alipbekov, A. S. Galkin, and S. Tulegenov, *Research of the Earth's Crust and Upper Mantle of Kazakhstan with Magnetotelluric Methods* (Nauka, Alma-Ata, 1977) [in Russian].
2. E. V. Artyushkov, *Geodynamics* (Nedra, Moscow, 1979) [in Russian].
3. E. V. Artyushkov, *Physical Tectonics* (Nauka, Moscow, 1993) [in Russian].
4. N. A. Bogdanov, "Tectonics of the Arctic Ocean," Geotectonics **38** (3), 166–181 (2004).
5. V. G. Bogolepov, N. A. Gulyaeva, D. A. Safin, et al., "Technique of orebody prospecting at the Akchatau rare-metal deposit (Central Kazakhstan)," in *Mineralogy and Geochemistry of Tungsten Deposits* (Nauka, Leningrad, 1975), pp. 55–65 [in Russian].
6. A. A. Borisov, *Deep Structure of the USSR Territory from Geophysical Data* (Nedra, Moscow, 1967) [in Russian].
7. N. K. Bulin and A. V. Egorkin, *Regional Forecasting of Subsurface Petroleum Resource Potential on the Basis of Deep Seismic Criteria* (GEON, Moscow, 2000) [in Russian].
8. Yu. I. Galushkin, *Simulation of Sedimentary Basins and Estimation of Their Petroleum Resource Potential* (Nauchnyi mir, Moscow, 2007) [in Russian].
9. Yu. I. Galushkin and Ya. B. Smirnov, "Thermal history of sedimentary basins: Express methods of heat flow estimation," Geol. Geofiz. **28** (11), 105–112 (1987).
10. Yu. I. Galushkin, Ya. B. Smirnov, A. Bertol'd, and G. Ol'szak, "Characterization of thermal history of the East Elba part of the Northwestern European Basin and the Dnieper–Donets Basin: Mechanism of development and estimation of localization of petroliferous zones," in *Plate Tectonics and Paleozoic Mineral Resources* (Nedra, Moscow, 1985), pp. 132–147 [in Russian].
11. V. A. Golubev, *Conductive and Convective Removal of Heat in the Baikal Rift Zone* (GEO, Novosibirsk, 2007) [in Russian].
12. A. Ya. Holmstock, "Effect of sedimentation on deep heat flow," Okeanologiya *19* (6), 1133–1138 (1979).
13. A. F. Grachev, E. R. Drubetskoi, M. A. Martynova, E. M. Prasolov, Yu. N. Dedenkov, A. A. Sukhanov, "First data on helium isotopic composition in rocks of the Baikal Rift and water of the Lake Baikal," in *Proceedings of the 9th All-Union Symposium on Stable Isotopes in Geochemistry, November 16–19, 1982, Moscow* (GEOKhI AN SSSR, Moscow, 1982), pp. 114–116 [in Russian].
14. D. H. Green and A. E. Ringwood, "Origin of calc-alkaline igneous rocks," in *Petrology of the Upper Mantle* (Australian National University, Canberra, 1966; Mir, Moscow, 1968), pp. 118–131.
15. K. E. Degtyarev, *Tectonic Evolution of the Early Paleozoic Island-Arc Systems and Formation of the Earth's Crust in the Caledonides of Kazakhstan* (GEOS, Moscow, 2012) [in Russian].
16. E. R. Drubetskoi and A. F. Grachev, "Basalts and ultramafic xenoliths in the Baikal Rift Zone: Helium and argon isotopes," in *Deep Xenoliths and Structure of the Lithosphere* (Nauka, Moscow, 1987), pp. 54–63 [in Russian].
17. A. D. Duchkov, L. S. Sokolova, Z. A. Solov'eva, and Z. S. Khaikovsky, "Heat flow in western part of the

Altai–Sayan region," Geol. Geofiz. **19** (4), 96–100 (1978).

18. A. N. Evdokimov, Volcanoes of Spitsbergen (VNIIOkeangeologiya, St. Petersburg, 2000) [in Russian].
19. L. P. Zonenshain, *Geosynclinal Concept and Its Application to the Central Asian Belt* (Nedra, Moscow, 1972) [in Russian].
20. V. G. Levashkevich, *Doctoral Dissertation in Geology and Mineralogy* (MGU, Moscow, 2005).
21. Yu. G. Leonov, "Continental rifting: Modern views, problems and solutions," Geotectonics, **35** (2), 81–92 (2001).
22. Yu. G. Leonov and M. D. Khutorskoi, "Orla (Storoya) Trench as an eleemnt of recent geodynamics in outer zone of Barents Sea shelf," in *Structure and Evolution of the Lithosphere* (Paulsen Editions, Moscow–St. Petersburg, 2010), pp. 158–175 [in Russian].
23. S. V. Lysak, *Heat Flow in Continental Rift Zones* (Nauka, Novosibirsk, 1988) [in Russian].
24. B. A. Mamyrin and I. N. Tolstikhin, *Helium Isotopes in Nature* (Energoizdat, Moscow, 1980) [in Russian].
25. A. A. Mossakovsky, *Orogenic Structures and Volcanism of Eurasian Paleozoides and Their Place in Formation of Continental Earth's Crust* (Nauka, Moscow, 1975) [in Russian].
26. A. A. Mossakovsky, S. V. Ruzhentsev, S. G. Samygin, and T. N. Kheraskova, "The Central Asian Foldbelt: Geodynamic evolution and formation history," Geotektonika **27** (6), 3–32 (1993).
27. E. E. Musatov, "Neotectonic structure," in *Geology and Mineral Resources of Russia, Vol. 5, Book 1: Arctic Seas* (VSEGEI, St. Petersburg, 2004), pp. 26–31 [in Russian].
28. N. V. Nevolin, V. M. Kovylin, G. A. Maslyaev, et al., *Geological and Geophysical Simulation of Petroliferous Territories* (Nedra, Moscow, 1993) [in Russian].
29. V. G. Nikolaev, *The Pannonian Basin: Structure of Sedimentary Cover and Evolution* (Nauka, Moscow, 1986) [in Russian].
30. *Sedimentary Basins: Research Methods, Structure and Evolution*, Ed. by Yu.G. Leonov and Yu.A. Volozh (Nauchnyi mir, Moscow, 2004) [in Russian].
31. *Sedimentary Cover of the World Ocean Bottom and Land from the Data of Seismic Survey* (Nauka, Moscow, 1984) [in Russian].
32. A. V. Peive and A. A. Saveliev, "Structure and movements in the Lithosphere," Geotektonika, **16** (6), 5–24 (1982).
33. A. V. Peive, N. A. Streis, A. A. Mossakovsky, et al., "Paleozoides of Eurasia and some questions of geosynclinal evolution," Sov. Geol., No. 12, 7–25 (1972).
34. A. V. Peive, A. L. Yanshin, L. P. Zonenshain, et al., "Formation of the continental Earth's crust in northern Eurasia in connection with compilation of a new tectonic map," Geotektonika **10** (5), 6–23 (1976).
35. A. S. Perfil'ev, *Formation of the Earth's Crust in the Ural Eugeosyncline* (Nauka, Moscow, 1979) [in Russian].
36. *Underwater Geological Research from Manned Submersibles* (Nauka, Moscow, 1985) [in Russian].
37. B. G. Polyak, *Heat and Mass Flow from the Mantle in Major Structural Units of the Earth's Crust* (Nauka, Moscow, 1988) [in Russian].
38. B. G. Polyak, "Spreading and rifting: Specific character of helium isotopic compositions," Geotectonics **38** (6), 19–32 (2004).
39. B. G. Polyak and Ya. B. Smirnov, "Relationship of deep heat flow to tectonic structure of continents," Geotectonics **2** (4), 3–19 (1968).
40. B. G. Polyak, V. I. Kononov, and M. D. Khutorskoi, "Heat flow and lithosphere structure of Iceland in the light of new evidence," Geotectonics **18** (1), 111–119 (1984).
41. B. G. Polyak, V. V. Gordienko, A. L. Cheshko, et al., "Helium isotopes, heat flow, and tectonics of the Eastern Carpathians," Dokl. Earth Sci. **367** (5), 732–737 (1999).
42. B. G. Polyak, V. Yu. Lavrushin, A. L. Cheshko, E. M. Prasolov, and I. L. Kamensky, "Recent tectonomagmatic reactivation of the Kolyuchino–Mechigmen Zone of the Chukchi Peninsula from data on the composition of gases in hydrothermal springs," Geotectonics **44** (6), 529–540 (2010).
43. B. G. Polyak, I. N. Tolstikhin, and V. P. Yakutseni, "Helium isotopic composition and heat flow: Geochemical and geophysical aspects of tectogenesis," Geotektonika **13** (5), 3–23 (1979).
44. A. K. Popova, Ya. B. Smirnov, and M. D. Khutorskoi, "Geothermal field of transform fracture zones," in *Deep faults of oceanic bottom* (Nauka, Moscow, 1984), pp. 78–87 [in Russian].
45. Yu. M. Pushcharovsky, "Preface," in *Continental and Oceanic Rifting* (Nauka, Moscow, 1985), pp. 3–4 [in Russian].
46. V. A. Romanov, *Tectonics of Magnitogorsk Megasynclinorium* (Inst. Geol., Ufa, 1985) [in Russian].
47. V. E. Sal'nikov, *Geothermal Regime of the South Urals* (Nauka, Moscow, 1984) [in Russian].
48. *Seismic Models of the Lithosphere in Major Geostructures in Territory of the USSR* (Nauka, Moscow, 1980) [in Russian].
49. F. Khorvath, L. Bodri, and P. Ottlik, "Geotermics of Hungary and tectonophysics of "red spot" in the Pannonian Basin," in *Thermal Field of Europe*, Ed. by V. Tschermak and L. Ribakh (Mir, Moscow, 1982), pp. 176–190 [in Russian].
50. M. D. Khutorskoi, "Heat flow, structure, and evolution model of the lithosphere in the South Urals and Central Kazakhstan," Geotektonika **19** (3), 77–88 (1985).
51. M. D. Khutorskoi, *Geothermics of the Central Asian Foldbelt* (RUDN, Moscow, 1996) [in Russian].
52. M. D. Khutorskoi, M. P. Antipov, Yu. A. Volozh, and B. G. Polyak, "Temperature field and a 3D geothermal model of the North Caspian Basin," Geotectonics **38** (1), 53–60 (2004).
53. M. D. Khutorskoi, K. G. Viskunova, L. V. Podgornykh, O. I. Suprunenko, and V. R. Akhmedzyanov, "A temperature model of the crust beneath the Barents Sea: Investigations along geotraverses," Geotectonics **42** (2), 36–54 (2008).

54. M. D. Khutorskoi, A. M. Gorodnitsky, A. Ya. Holmstock, et al., "Heat flow, basaltic volcanism, and structure of the lithosphere in the Tyrrhenian Sea," Geotektonika **20** (5), 116–123 (1986).
55. M. D. Khutorskoi, L. V. Podgornykh, I. S. Gramberg, and Yu. G. Leonov, "Thermal tomography of the West Arctic Basin," Geotectonics **37** (3), 79–96 (2003).
56. M. D. Khutorskoi, Yu. G. Leonov, A. V. Ermakov, and V. R. Akhmedzyanov, "Abnormal heat flow and the trough's nature in the Northern Svalbard Plate," Dokl. Earth Sci. **424** (1), 29–35. (2009).
57. M. D. Khutorskoi, E. A. Teveleva, L. A. Tsybulya, and G. I. Urban, "Heat flow in salt-dome basins of Eurasia: A comparative study," Geotectonics **44** (4), 289–304 (2010).
58. A. M. Sengör and B. A. Natal'in, *Rifts of the World* (GEOKART, Moscow, 2009) [in Russian].
59. V. A. Shchapov, A. K. Yurkov, D. Yu. Demezhko, and V. V. Nikolaev, "Geothermal study of the Ural Superdeep," in *Thermal Field of the Earth and Research Methods* (RUDN, Moscow, 1997), pp. 195–198 [in Russian].
60. F. Barberi, H. Bizonard, G. Ferrara, P. Gasparini, et al., "Age and nature of basalts from the Tyrrhenian abyssal plain," in *DSDP Initial Rep. Leg. 42* (1978), Site 373a, pp. 509–513.
61. F. Birch, R. F. Roy, and E. R. Decker, "Heat flow and thermal history in New England and New York," in *Studies in Appalachian Geology* (American Monography, New York, 1968), Chapter 33, pp. 437–451.
62. D. K. Blackman, J. A. Karson, D. S. Kelley, J. R. Cann, G. L. Fruh-Green, J. S. Gee, S. D. Hurst, B. E. John, J. Morgan, S. L. Nooner, D. K. Ross, T. J. Schroeder, and E. A. Williams, "Geology of the Atlantis Massif (MAR 30 N): Implications for the evolution of an ultramafic oceanic core complex," Mar. Geophys. Res. **23**, 443–469 (2004).
63. M. Boccaletti, F. Horvath, M. Loddo, et al., "The Tyrrhenian and Pannonian basins: A Comparison of two Mediterranean interarc basins," Tectonophysics **35**, 45–69 (1976).
64. M. Boccaletti, R. Nicolich, and L. Tortorici, "The Calabrian Arc and the Ionian Sea in the dynamic evolution of the Central Mediterranean," Mar. Geol. **55**, 219–245 (1984).
65. E. Bonatti, K. Hartman, F. Innocenti, and R. Kay, "Basalt drilled at the Vema Fracture Zone," in *DSDP Initial Rep. Leg 39* (1977), pp. 507–511.
66. I. Cornides, N. Takaoka, K. Nagao, and S. Matsuo, "Contribution of mantle-derived gases to subsurface gases in a tectonically quiescent area, the Carpathian Basin, Hungary, revealed from noble gases measurements," Geochem. J. **20**, 119–125 (1986).
67. B. Della Vedova, G. Pollis, I. P. Foucher, and J. P. Rehault, "Geothermal structure of the Tyrrhenian Sea," Mar. Geol. **55**, 271–289 (1984).
68. R. A. Folinsbee, Heat flow over the equatorial Mid-Atlantic Ridge, *Degree Master of Sci. Dissertation,* Massachusetts Inst. Technology, 68 (1969).
69. E. Griesshaber, R. K. O' Nions, and E. R. Oxburgh, "Helium and carbon isotope systematics in crustal fluids from the Eifel, the Rhine Graben and Black Forest, F.R.G," Chem. Geol. **99**, 213–235 (1992).
70. I. Hutchinson, "The effect of sedimentation and compaction on oceanic heat flow," Geophys. Roy. Astron. Soc. **82**, 439–459 (1985).
71. C. Jaupart, J. G. Sclater, and G. Simmons, "Heat flow studies: Constraints on the distribution of uranium, thorium, and potassium in the continental crust," Earth Planet. Sci. Lett. **52**, 328–344 (1981).
72. I. T. Kukkonen, I. V. Golovanova, Yu. V. Khachay, et al., "Low geothermal heat flow of the Urals Fold Belt - implication of low heat production, fluid circulation, or palaeoclimate?" Tectonophysics **276**, 63–85 (1997).
73. A. H. Lachenbruch, "Preliminary geothermal model of the Sierra Nevada," J. Geophys. Res. **73**, 6977–6989 (1968).
74. A. H. Lachenbruch and J. H. Sass, "Heat flow and energetics of the San Andreas Fault Zone," J. Geophys. Res. **85** (B11), 6185–6222 (1980).
75. M. Langseth and M. Hobart, "Interpretation of heat flow measurements in the Vema Fracture Zone," Geophys. Rev. Lett. **3** (5), 241–244 (1974).
76. L. Lenkey, *Geothermics of the Pannonian Basin and Its Bearing on the Tectonics of Basin Evolution* (Netherlands Research School of Sedimentary Geology, Amsterdam, 1999).
77. D. P. McKenzie, "The variation of temperature with time and hydrocarbon maturation in sedimentary basins formed by extension," Earth Planet. Sci. Lett. **55**, 87–98 (1981).
78. B. Marty and I. N. Tolstikhin, "CO_2 fluxes from mid-oceanic ridges, arcs, and plumes," Chem. Geol. **145**, 233–248 (1998).
79. R. A. Mohr, "The Cenozoic volcanic succession in Ethiopia," Bull. Volcanol. **32** (1), 5–14 (1968).
80. E. R. Oxburgh, R. K. O' Nions, and R. I. Hill, "Helium isotopes in sedimentary basins," Nature **324** (3/4), 632–635 (1986).
81. J. P. Rehault, J. Mascle, A. Fabbri, et al., "The Tyrrhenian Sea before Leg 107," in *ODP Initial Report. Leg 107* (1987), pp. 9–35.
82. R. F. Roy, E. R. Decker, D. D. Blackwell, and F. Birch, "Heat flow in the United States," J. Geophys. Res. **73** (16), 5202–5221 (1968).
83. A. M. C. Sengör and K. Burke, "Relative timing of rifting and volcanism on the Earth and its tectonic implication," Geophys. Rev. Lett. **5**, 419–421 (1978).
84. *The Pannonian Basin, a Study in Basin Evolution*, Ed. by L. H. Royden and F. Horvath (AAPG Mem., 1988), Vol. 45.
85. T. H. Van Andel, J. Thiede, J. G. Sclater, and W. W. Hay, "Depositional history of the South Atlantic ocean during the last 125 million years," J. Geol. **85** (6), 651–698 (1977).
86. D. Williams, K. Green, T. van Andel, et al., "The hydrothermal mounds of the Galapagos Rift: Observations with DSRV "Alvin" and detailed heat flow studies," J. Geophys. Res. **84** (B13), 85–100 (1979).

Reviewers: Yu.G. Leonov and V.N. Puchkov

Translated by V. Popov

SPELL: 1. Shchapov, 2. Demezhko, 3. Superdeep